UC Davis

UC Davis Previously Published Works

Title

CO2 Hydrogenation on Ni(100): Effect of Reaction Conditions on the Adsorption Sites of CO Intermediates and the Chemical State of Nickel

Permalink

https://escholarship.org/uc/item/5vn9942z

Journal

The Journal of Physical Chemistry C, 130(31)

ISSN

1932-7447

Authors

David, Roey Ben

Akerman, Michelle Sykes

Kim, Dongwoo

et al.

Publication Date

2026-08-06

DOI

10.1021/acs.jpcc.6c04216

Copyright Information

This work is made available under the terms of a Creative Commons Attribution License, available at https://creativecommons.org/licenses/by/4.0/

Peer reviewed

eScholarship.org Powered by the California Digital Library
University of California

THE JOURNAL OF PHYSICAL CHEMISTRY C
A JOURNAL OF THE AMERICAN CHEMICAL SOCIETY

Open Access
This article is licensed under CC-BY 4.0

pubs.acs.org/JPCC
Article

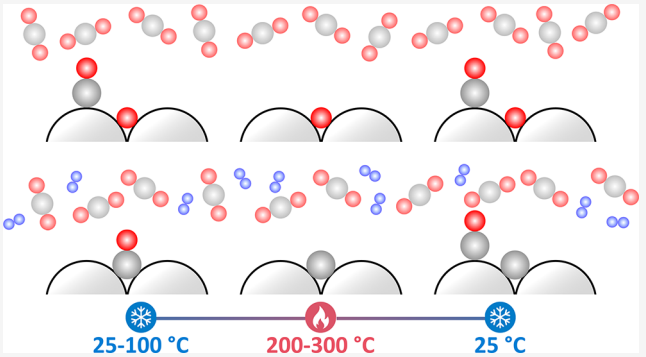
CO_2 Hydrogenation on Ni(100): Effect of Reaction Conditions on the Adsorption Sites of CO Intermediates and the Chemical State of Nickel

Roey Ben David, Michelle Sykes Akerman, Dongwoo Kim, Slavomír Nemšák, and Baran Eren*

Cite This: J. Phys. Chem. C 2026, 130, 10952−10957
Read Online

ACCESS | Metrics & More | Article Recommendations | Supporting Information

ABSTRACT: Adsorbed CO is a key intermediate in CO_2 hydrogenation on Ni-based catalysts because its stability and adsorption site influence the competition between the reverse water−gas shift reaction and CO_2 methanation. Here we use in situ infrared spectroscopy and ambient-pressure X-ray photoelectron spectroscopy to follow the evolution of CO* intermediates and the chemical state of Ni(100) under CO_2 and H_2 between 25 and 300 °C. We show that the adsorption site of CO depends strongly on coadsorbed atomic species (O*, H*, and C*). Under CO_2, CO adsorbs mainly on top sites, whereas H_2 removes surface oxygen and stabilizes bridge-bonded CO at low temperature. At higher temperature, H_2 promotes CO dissociation, leading to atomic carbon and Ni carbide that create new adsorption sites for CO. These findings show that H_2 plays a central role in enabling complete CO_2 dissociation on Ni(100) and in controlling the adsorption site and stability of CO intermediates. These findings also demonstrate that the reaction pathway on Ni(100) differs from that on Ni(111).



INTRODUCTION

CO_2 hydrogenation has attracted broad interest as a route for carbon utilization and the production of fuels and value-added chemicals.[1,2] Nickel-based catalysts are active for both the reverse water−gas shift (RWGS) reaction[2,3] and CO_2 methanation,[4,5] which determine whether CO or methane is the dominant product. Selectivity between these pathways depends strongly on reaction conditions and catalyst structure, making a molecular-level understanding of facet-dependent reactivity and surface dynamics essential.[6−8]

In both RWGS and CO_2 methanation, CO is a key intermediate that can either desorb or undergo further dissociation and hydrogenation.[6,7] Its reactivity depends strongly on its adsorption site, which in turn depends on surface structure and coadsorbed species.[9−13] Under reaction conditions, Ni surfaces are dynamic and are continuously modified by species formed by CO_2 and H_2 dissociation.[8,12,14] These species can occupy surface and subsurface sites, alter the electronic structure of the catalyst, and change the availability and nature of adsorption sites for CO.

In our previous works on Ni(111), we showed that atomic oxygen determines the adsorption site of CO formed in the first step of CO_2 dissociation.[12,13] On Ni(100), however, CO can also dissociate further to C* and O*,[15] which makes the surface chemistry more complex.[14] Although the surface chemistry of Ni(100) under different reaction conditions has been studied extensively,[14,16] a direct correlation between the evolving surface composition and the adsorption site of CO intermediates is still missing.

Here we examine how reaction conditions control both the adsorption site of CO* and the chemical state of Ni(100). By combining in situ polarization-modulation infrared reflection−absorption spectroscopy (PM-IRRAS) and ambient-pressure X-ray photoelectron spectroscopy (AP-XPS), we follow the evolution of adsorbed CO and coadsorbed atomic species under CO_2 and H_2 between 25 and 300 °C. The results show that the CO adsorption site is dynamically controlled by O*, H*, and C*, whose relative stability depends strongly on temperature and gas composition. We further show that removal of surface oxygen by hydrogen is a key step that enables CO* activation and C* formation on Ni(100). This activation is a crucial step in the carbide reaction pathway for CO_2 methanation.

Received: June 26, 2026
Revised: July 10, 2026
Accepted: July 16, 2026
Published: July 25, 2026



Downloaded from pubs.acs.org/jpccck/article-pdf/130/31/10952/6254925/acs.jpcc.6c04216.pdf by guest on 11 November 2026

ACS Publications
© 2026 The Authors. Published by American Chemical Society

https://doi.org/10.1021/acs.jpcc.6c04216
J. Phys. Chem. C 2026, 130, 10952−10957

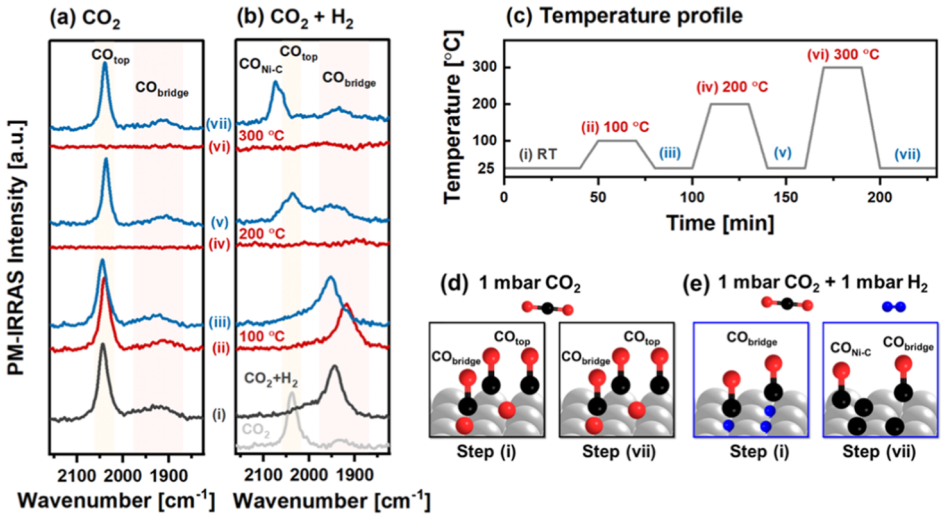


Figure 1. PM-IRRAS spectra of Ni(100) under (a) 1 mbar CO_2 and (b) 1 mbar CO_2 + 1 mbar H_2. In both experiments, CO_2 and H_2 were dosed at 25 °C, and the surface was then heated and cooled according to the sequence shown in (c). Schematics of the surface intermediates and CO* adsorption sites at steps (i) and (vii) are shown in (d) for CO_2 and in (e) for CO_2 + H_2.

EXPERIMENTAL SECTION

PM-IRRAS experiments were performed in a UHV system consisting of a load-lock, a preparation chamber, and an IR measurement chamber. A detailed description of operation in UHV and ambient-pressure modes is available elsewhere.[17,18] The preparation chamber (base pressure 1−3 × 10^{-10} mbar) was used to clean the Ni(100) single-crystal surface (⌀14 mm, thickness = 2 mm, MaTeck GmbH) by repeated Ar^+ sputtering (1.5 kV, 5 mA, 20−30 min) and annealing (25 min at 650 °C). After preparation, the crystal was transferred through a gate valve into the PM-IRRAS chamber (base pressure ≤1 × 10^{-10} mbar), which was equipped with a Nicolet iS50 FTIR spectrophotometer. Before each gas-dosing experiment, a reference PM-IRRAS spectrum was recorded at RT in UHV to verify surface cleanliness and to subtract the Bessel-function curvature from subsequent spectra. CO_2 and H_2 (Airgas USA, 99.999% and 99.9999%, respectively) were introduced through manual leak valves in static-pressure mode at room temperature (RT) ∼25 °C, and PM-IRRAS spectra were collected as a function of time and/or temperature according to the heating profiles described in the main text (25 °C ≤ T ≤ 300 °C). The sample was resistively heated from the back via Prevac's stainless steel PTS800 sample holders. Each spectrum shown here represents an average of 1500 scans to improve the signal-to-noise ratio. Between ambient-pressure experiments, the analysis chamber was baked for at least 24 h at 120 °C to restore the base pressure, and the Ni(100) crystal was recleaned by 5−10 additional sputtering and annealing cycles.

Supplementary AP-XPS measurements were performed at beamline 9.3.2 of the Advanced Light Source (ALS),[19] equipped with a VG-Scienta R4000 HiPP hemispherical electron analyzer (Scienta, now Scienta Omicron) operated with a pass energy of 100 eV. This beamline provides a lower flux density (5 × 10^7−2 × 10^8 photons cm^{-2} s^{-1}) than most AP-XPS beamlines, which reduces beam-induced effects.[20] Photon energies of 430 eV for C 1s and 680 eV for O 1s were chosen to give a photoelectron kinetic energy of about 150 eV. Ni 3p region was also measured with 430 eV photons. Before the measurements, the same Ni(100) sample used in the IR experiments was cleaned by more than 10 cycles of conventional Ar^+ sputtering (1.5 kV) followed by annealing at 650 °C. The base pressures in the preparation and measurement chambers were approximately 5 × 10^{-9} and 3 × 10^{-9} mbar, respectively. The measurement chamber was baked before the experiments and reached a base pressure of 2 × 10^{-10} mbar; however, the pressure increased after initial test exposures to CO_2 conducted before the measurements reported here. Because the sample had previously been exposed to CO_2 at elevated temperature during the IR experiments, it contained a relatively high concentration of dissolved oxygen. As in the IR experiments, CO_2 and H_2 (PRAXAIR, now Linde; 99.999% and 99.9999%, respectively) were dosed through leak valves. Because of the tendency to form carbonates,[16,21] AP-XPS measurements were carried out only above 100 °C, with H_2 dosed before CO_2. The sample was resistively heated from the back via a Pt wire. All binding energies were calibrated to the Fermi level measured at the same photon energy. Spectra were fitted with a combination of symmetric and asymmetric Gaussian−Lorentzian line shapes after background subtraction.

RESULTS AND DISCUSSION

We first used in situ PM-IRRAS to examine how temperature affects the adsorption site of the CO* intermediate under CO_2 and CO_2 + H_2. Figure 1a,b show spectra collected under 1 mbar CO_2 and 1 mbar CO_2 + 1 mbar H_2, respectively, using the heating sequence in Figure 1c. For Ni(100) in CO_2 at 25 °C (Figure 1a(i)), the PM-IRRAS spectrum shows an intense band at 2043 cm^{-1} and a weaker, broader band at 1922 cm^{-1}, assigned to CO adsorbed on top sites (CO_{top}) and bridge sites (CO_{bridge}), respectively.[22−24] These peaks appear because CO_2 dissociatively adsorbs on Ni(100) to produce CO* and O*. Although O* species (Ni−O vibrations below 650 cm^{-1}) are not detected in the present PM-IRRAS setup, previous studies showed that atomic oxygen preferentially occupies 4-fold hollow sites on Ni(100).[25,26] When the temperature is increased to 100 °C (step (ii) in Figure 1a), both CO_{top} and CO_{bridge} shift slightly to lower wavenumber, consistent with lower surface coverage. At 200 and 300 °C (steps (iv) and (vi)), both bands disappear because CO* desorbs completely from the surface. The short residence time of CO* formed by

Downloaded from pubs.acs.org/jpccck/article-pdf/130/31/10952/6254925/acs.jpcc.6c04216.pdf by guest on 11 November 2026

https://doi.org/10.1021/acs.jpcc.6c04216
J. Phys. Chem. C 2026, 130, 10952−10957

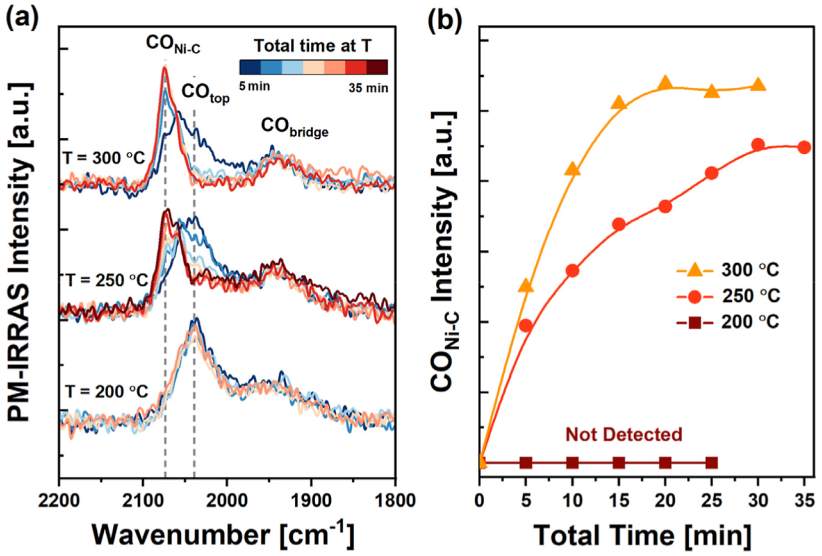


Figure 2. (a) PM-IRRAS spectra of Ni(100) after heating−cooling cycles under 1 mbar CO_2 + 1 mbar H_2 at 200, 250, and 300 °C. In each cycle, the sample was heated to the selected temperature for 5 min and then cooled to RT. All spectra were recorded at RT and are plotted against the total annealing time. (b) Intensity of the CO_{Ni-C} peak (~2073 cm^{-1}) as a function of accumulated annealing time at each temperature. The 2073 cm^{-1} peak borrows intensity from the 2060 cm^{-1} peak, a purely physical (nonchemical) effect; therefore, the trend is a nonlinear measure of CO_{Ni-C} coverage.

CO_2 dissociation at these temperatures (T ≥ 200 °C) agrees with previous thermal desorption studies.[23,27]

The spectra recorded after cooling the sample back to RT (steps (iii), (v), and (vii) in Figure 1a) provide information on changes in surface chemistry during heating, especially on the distribution of CO* over different adsorption sites after cooling.[12,13] In CO_2 (Figure 1a), the CO_{top} and CO_{bridge} bands measured at RT are essentially unchanged after heating to different temperatures and cooling back, as illustrated in Figure 1d. This behavior contrasts with that of Ni(111), where CO* and O* compete for the same energetically preferred adsorption sites, namely the 3-fold hollow sites. As a result, the accumulation of O* during annealing at elevated temperatures significantly affects the site distribution of CO*.[13] On Ni(100), however, O* and CO* preferentially occupy different adsorption sites. Consequently, the accumulation of O* upon annealing has little effect on either the distribution or the coverage of adsorbed CO. Nevertheless, the slight red shift of the CO_{bridge} band from 1922 cm^{-1} before heating (Figure 1a(i)) to 1912 cm^{-1} after annealing at 300 °C and cooling back to RT (Figure 1a(vii)) may indicate a modest influence of accumulated O* on the adsorption environment of CO. In contrast to pure CO_2, clear temperature-dependent changes are observed under CO_2 + H_2 (Figure 1b). Already at RT (step (i)), adding 1 mbar H_2 to 1 mbar CO_2 shifts the preferred adsorption site of CO* from top (2038 cm^{-1}) to bridge (1944 cm^{-1}). We attribute this site shift to two consecutive processes: (1) removal of oxygen from 4-fold hollow sites through reaction with H*, a product of dissociative H_2 adsorption, to form OH and H_2O, and (2) further dissociative adsorption of H_2, which places H* in 4-fold hollow sites.[28] As shown previously for Ni(100) under CO and H_2[24], coadsorbed H* stabilizes CO on bridge sites through electronic effects.[29,30] This H-stabilized CO_{bridge} configuration is illustrated in Figure 1e(i). By contrast, at high coverage and in the absence of coadsorbates, CO on Ni(100) preferentially occupies top sites at RT.[23]

After heating the sample to 100 °C under 1 mbar CO_2 + 1 mbar H_2 (step (ii) in Figure 1b), the CO_{bridge} peak red-shifts from 1944 to 1919 cm^{-1} as the CO* coverage decreases. At 200 and 300 °C (steps (iv) and (vi)), only very weak, broad features remain because the CO* coverage is low and thermal broadening is significant.[31] No major change is observed after cooling from 100 °C to RT (step (iii)). In contrast, annealing at 200 and 300 °C leads to pronounced changes in the RT spectra (steps (v) and (vii)). After annealing at 200 °C, the CO_{bridge} peak near 1947 cm^{-1} decreases in intensity and the CO_{top} peak at 2036 cm^{-1} reappears. This reappearance indicates that H*, which stabilizes bridge-bound CO, is no longer the dominant species in the 4-fold hollow sites of Ni(100). One possible adsorbate on these sites after heating is atomic oxygen. As we showed previously for CO_2 + H_2 on Ni(111),[12] oxygen that penetrates into subsurface layers at 200 °C can act as a reservoir that affects the CO adsorption site after cooling. Here, however, the combined PM-IRRAS and AP-XPS data point instead to site occupation by atomic carbon. Atomic carbon on Ni(100) at elevated temperature may form through CO* dissociation (CO* → C* + O*) or CO* disproportionation (2CO* → C* + CO_2).[15] Like oxygen, carbon preferentially occupies the 4-fold hollow sites of Ni(100), but its adsorption energy is substantially higher than that of oxygen or hydrogen, making it the more stable surface species.[32] A previous IR study also showed that atomic carbon on Ni(100) favors the coadsorption of CO at top sites.[24]

Heating the surface to 300 °C leads to additional changes in the PM-IRRAS spectrum measured after cooling to RT (step (vii) in Figure 1b). The CO_{bridge} peak decreases further relative to step (v), and a new CO stretching band appears at 2073 cm^{-1} with a shoulder near 2060 cm^{-1}. The band near 2060 cm^{-1} can be assigned to CO_{top} blue-shifted by dissolved subsurface carbon, whereas the higher-frequency band is assigned to CO adsorbed on a carbidic Ni site (CO_{Ni-C}).[24] The formation of dissolved carbon and a Ni carbide layer can be explained by atomic carbon generated by CO* decom-

Downloaded from pubs.acs.org/jpccck/article-pdf/130/31/10952/6254925/acs.jpcc.6c04216.pdf by guest on 11 November 2026

https://doi.org/10.1021/acs.jpcc.6c04216
J. Phys. Chem. C 2026, 130, 10952−10957

position or disproportionation and its subsequent accumulation in the subsurface region. The adsorption of CO on carbidic Ni sites after heating to 300 °C is illustrated in Figure 1e(vii).

The kinetics of Ni carbide formation under CO_2 + H_2 were examined by temperature-cycling experiments between RT and temperatures in the 200−300 °C range (Figure 2). In each experiment, the sample was heated to the selected temperature for 5 min, then cooled to RT, and PM-IRRAS spectra were recorded as a function of total annealing time (Figure 2a). The intensity of the CO_{Ni}−$_C$ peak at ∼2073 cm^{-1} was used to monitor the growth of the Ni carbide layer (Figure 2b). After annealing cycles at 200 °C, the CO_{Ni}−$_C$ peak was not detected for annealing times up to 25 min, and the CO_{top} and CO_{bridge} bands remained unchanged. At this temperature, the surface is therefore consistent with adsorbed atomic carbon and oxygen but not with a continuous carbide layer. After annealing cycles at 250 °C, the CO_{Ni}−$_C$ peak increases clearly with time, together with a blue shift and loss of intensity of the CO_{top} peak; the process is even faster at 300 °C. These results indicate rapid growth of a Ni carbide layer on Ni(100) under CO_2 + H_2 above 250 °C. In stark contrast to Ni(100), no such changes take place on Ni(111), on which no significant CO_{Ni}−$_C$ band is detected after annealing at 300 °C.[12] Thus, the reaction pathway of CO_2 hydrogenation on Ni is highly structure sensitive.

To verify the assignment of the 2073 cm^{-1} band to CO_{Ni}−$_C$, we performed complementary AP-XPS measurements, which can directly probe carbide formation. No prominent C 1s features are observed in UHV or in H_2, but peaks associated with CO_2 dissociation appear when both gases are present, as shown in Figure 3. At 100 °C, the main feature is a peak at about 285.6 eV, assigned to CO*.[14] Its slight asymmetry is partially due to vibrational losses and partially due to a small amount of carbonate contamination. Less intense features are also present: a peak at 283.0 eV due to sp-hybridized carbon and a peak at 284.2 eV assigned to sp^2-hybridized carbon

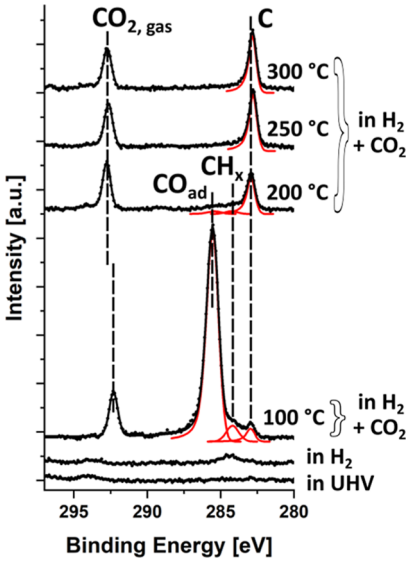


Figure 3. C 1s region of the AP-XPS spectra obtained in UHV at RT, in 0.075 mbar H_2 at RT, and in 0.075 mbar H_2 + 0.075 mbar CO_2 at 100, 200, 250, and 300 °C. Black dots are the experimental data, the solid black line is the fit, and the red lines mark the peaks discussed in the main text. The spectra are shown after background subtraction.

(CH_x), which is associated with either aliphatic hydrocarbon contamination or graphitized carbon.[33,34] Because of the sample history, the sample initially contains a relatively high concentration of dissolved oxygen, as seen in the O 1s spectra in Figure S1. At 100 °C, however, the intensity of the dissolved-oxygen signal near 530.0 eV does not change significantly, apart from a small decrease caused by gas-phase attenuation. The O 1s counterpart of the 285.6 eV CO* peak is not used in the analysis because it overlaps with the OH* contribution at 531.5 eV. The OH* feature itself arises from hydroxylation during the initial H_2 dosing, both because H_2 introduces residual water vapor to the surface and because it reacts with surface and dissolved oxygen to form hydroxyl species.

At 200 °C and above, the C 1s region changes substantially. At 200 °C, both the CO* and CH_x peaks decrease strongly in intensity, and at 250 and 300 °C they fall below the detection limit. In parallel, the sp-hybridized carbon peak increases at 200 °C and continues to grow as the temperature is raised. Its position also shifts slightly, from 283.0 eV at 200 °C to 282.8 eV at 250 and 300 °C, which is consistent with conversion of atomic surface carbon into a carbide layer, in agreement with the PM-IRRAS analysis. A similar negative shift of the sp-hybridized C 1s peak was reported for Ni(111) under related reaction conditions, although its origin was not discussed.[21] When the C 1s region is measured with 680 eV photons instead of 490 eV photons, giving lower surface sensitivity (Figure S2), the peak remains close to 283.0 eV even at 250 and 300 °C. This result suggests that the carbide layer is mainly confined to the surface, possibly in a reconstructed form, whereas the subsurface contains primarily dissolved atomic carbon. The dissolved-oxygen peak in the O 1s region (Figure S1) also decreases above 250 °C, consistent with partial replacement of dissolved oxygen by dissolved carbon. The atomic-carbon peak is slightly asymmetric because it is hybridized with metallic Ni. No clear change is observed in the Ni 3p spectra (Figure S1), which remain about 97% metallic (including carbidic Ni) and 3% oxidic under all conditions studied. This is expected because carbidic and metallic Ni have been reported to appear very similar in the Ni 3p region.[35]

Taken together, the PM-IRRAS and AP-XPS results support the formation of C* and Ni carbide during reaction of CO_2 and H_2 on Ni(100) at elevated temperature (T ≥ 200 °C). The data indicate that H_2 promotes complete CO_2 activation not only by removing O* through H_2O formation, but also by enabling subsequent CO* dissociation and carbon accumulation. This carbon modifies both the chemical state of the surface and the adsorption site of CO*. The interpretation is consistent with the additional PM-IRRAS experiments in Figures S3 and S4, which show that reversing the dosing order or increasing the H_2 partial pressure (1:10 partial pressure ratio) still leads to CO_{Ni}−$_C$ formation after reaction at elevated temperatures. Figures S3 and S4 also discuss respectively the further effects of reversing the dosing order and increasing the H_2 partial pressure. In both cases, the differences in spectral features compared to those presented here arise from a higher H* coverage (either due to H_2 predosing or due to higher H_2 partial pressure) which favors CO adsorption at bridge sites.

CONCLUSIONS

Using in situ PM-IRRAS and AP-XPS under mbar pressures of CO_2 and H_2, we show that the adsorption site of CO on Ni(100) is controlled by the relative stability of coadsorbed

Downloaded from pubs.acs.org/jpccck/article-pdf/130/31/10952/6625492/acs.jpcc.6c04216.pdf by guest on 11 November 2026

https://doi.org/10.1021/acs.jpcc.6c04216
J. Phys. Chem. C 2026, 130, 10952−10957

O*, H*, and C*. Under CO_2, oxygen causes CO adsorption mainly at top sites. Adding H_2 removes oxygen through H_2O formation and stabilizes bridge-bound CO at low temperature through coadsorbed H*. At higher temperature (T ≥ 200 °C), H_2 also enables CO* dissociation, leading to atomic carbon and eventually Ni carbide, which shift CO adsorption toward top and carbidic Ni sites. These results identify oxygen removal from the 4-fold hollow sites as the key step that enables H_2-assisted CO activation on Ni(100) and provide a mechanistic basis for controlling CO_2 hydrogenation pathways on Ni-based catalysts through reaction conditions. These results also show that CO_2 hydrogenation reaction pathways on Ni(100) and Ni(111) are fundamentally different, as the former both involves CO activation and change of CO intermediate sites.

■ ASSOCIATED CONTENT

Supporting Information

The Supporting Information is available free of charge at https://pubs.acs.org/doi/10.1021/acs.jpcc.6c04216.

O 1s and Ni 3p regions, and the C 1s region measured at a higher photon energy. Fitting parameters of the XPS. PM-IRRAS spectra with H_2 + CO_2 dosing (reversed dosing order) and with H_2-rich conditions (1:10 CO_2 to H_2 ratio) (PDF)

■ AUTHOR INFORMATION

Corresponding Author

Baran Eren − *Department of Chemical and Biological Physics, Weizmann Institute of Science, 76100 Rehovot, Israel; Fritz Haber Institute of the Max Planck Society, 14195 Dahlem, Berlin, Germany;* orcid.org/0000-0002-0521-8127; Email: baran.eren@weizmann.ac.il, eren@fhi.mpg.de

Authors

Roey Ben David − *Department of Chemical and Biological Physics, Weizmann Institute of Science, 76100 Rehovot, Israel*

Michelle Sykes Akerman − *Department of Chemical and Biological Physics, Weizmann Institute of Science, 76100 Rehovot, Israel*

Dongwoo Kim − *Advanced Light Source, Lawrence Berkeley National Laboratory, Berkeley, California 94720, United States*

Slavomír Nemšák − *Advanced Light Source, Lawrence Berkeley National Laboratory, Berkeley, California 94720, United States;* orcid.org/0000-0002-6103-2925

Complete contact information is available at: https://pubs.acs.org/10.1021/acs.jpcc.6c04216

Notes

The authors declare no competing financial interest.

■ ACKNOWLEDGMENTS

This research was supported by the Israel Ministry of Energy and Infrastructure and used resources of the Advanced Light Source, a U.S. DOE Office of Science User Facility under contract no. DE-AC02-05CH11231. B.E. acknowledges support by the Alexander von Humboldt Foundation.

■ REFERENCES

(1) Alper, E.; Yuksel Orhan, O. CO_2 Utilization: Developments in Conversion Processes. *Petroleum* **2017**, *3* (1), 109−126.

(2) Whang, H. S.; Lim, J.; Choi, M. S.; Lee, J.; Lee, H. Heterogeneous Catalysts for Catalytic CO_2 Conversion into Value-Added Chemicals. *BMC Chem. Eng.* **2019**, *1* (1), 1−19.

(3) Cao, X.; Han, Y. F.; Peng, C.; Zhu, M. A Review on the Water-Gas Shift Reaction over Nickel-Based Catalysts. *ChemCatChem* **2022**, *14* (16), e202200190.

(4) Vogt, C.; Monai, M.; Kramer, G. J.; Weckhuysen, B. M. The Renaissance of the Sabatier Reaction and Its Applications on Earth and in Space. *Nat. Catal.* **2019**, *2* (3), 188−197.

(5) Medina, O. E.; Amell, A. A.; López, D.; Santamaría, A. Comprehensive Review of Nickel-Based Catalysts Advancements for CO_2 Methanation. *Renew. Sustain. Energy Rev.* **2025**, *207*, 114926.

(6) Vogt, C.; Groeneveld, E.; Kamsma, G.; Nachtegaal, M.; Lu, L.; Kiely, C. J.; Berben, P. H.; Meirer, F.; Weckhuysen, B. M. Unravelling Structure Sensitivity in CO_2 Hydrogenation over Nickel. *Nat. Catal.* **2018**, *1* (2), 127−134.

(7) Sterk, E. B.; Nieuwelink, A. E.; Monai, M.; Louwen, J. N.; Vogt, E. T. C.; Filot, I. A. W.; Weckhuysen, B. M. Structure Sensitivity of CO_2 Conversion over Nickel Metal Nanoparticles Explained by Micro-Kinetics Simulations. *J. Am. Chem. Soc.* **2022**, *2* (12), 2714−2730.

(8) González, J. M.; Sabadell-Rendón, A.; Kaźmierczak, K.; Euzenat, F.; Montroussier, N.; Curulla-Ferré, D.; López, N. Nickel Dynamics Switches the Selectivity of CO_2 Hydrogenation. *Angew. Chem.* **2025**, *137* (5), e202417392.

(9) Chiarello, G.; Cupolillo, A.; Giallombardo, C.; Agostino, R. G.; Formoso, V.; Pacilè, D.; Papagno, L.; Colavita, E. Co-Adsorption of Oxygen and Carbon Monoxide on Ni(111). *Surf. Sci.* **2003**, *536* (1−3), 33−44.

(10) Braun, W.; Steinrück, H. P.; Held, G. The Surface Geometry of Carbonmonoxide and Hydrogen Co-Adsorbed on Ni{1 1 1}. *Surf. Sci.* **2005**, *574* (2−3), 193−204.

(11) Diesen, E.; Rodrigues, G. L. S.; Luntz, A. C.; Abild-Pedersen, F.; Pettersson, L. G. M.; Voss, J. Accuracy of XAS Theory for Unraveling Structural Changes of Adsorbates: CO on Ni(100). *AIP Adv.* **2020**, *10* (11), 115014.

(12) David, R. B.; Andres, M. A.; Shalom, B.-O.; Karagoz, B.; Held, G.; Eren, B. Atomistic Insights into the Surface Dynamics of Ni(111) during Reverse Water Gas Shift Reaction. *ChemCatChem* **2024**, *16* (20), e202400937.

(13) Ben David, R.; Head, A. R.; Lin, S.; Ben Yaacov, A.; Andres, M. A.; Eren, B. Molecular-Level Insights into CO_2 Activation on Ni(111) from in Situ Infrared Spectroscopy. *Cell Reports Phys. Sci.* **2024**, *5*, 101890.

(14) Lee, K. J.; Ye, Y.; Su, H.; Mun, B. S.; Crumlin, E. J. Correlating the Reverse Water-Gas Shift Reaction with Surface Chemistry: The Influence of Reactant Gas Exposure to Ni(100). *ACS Catal.* **2023**, *13* (13), 9041−9050.

(15) Keim, E. G.; Labohm, F.; Gijzeman, O. L. J.; Bootsma, G. A.; Geus, J. W. The Adsorption and Decomposition of Carbon Monoxide on Ni(100) and the Oxidation of the Surface Carbide by Oxygen. *Surf. Sci.* **1981**, *112* (1−2), 52−62.

(16) Cai, J.; Han, Y.; Chen, S.; Crumlin, E. J.; Yang, B.; Li, Y.; Liu, Z. CO_2 Activation on Ni(111) and Ni(100) Surfaces in the Presence of H_2O: An Ambient-Pressure X-Ray Photoelectron Spectroscopy Study. *J. Phys. Chem. C* **2019**, *123* (19), 12176−12182.

(17) Ben David, R.; Ben Yaacov, A.; Eren, B. Effect of Surface Orientation on Methanol Adsorption and Thermally Induced Structural Transformations on Copper Surfaces. *J. Phys. Chem. C* **2021**, *125* (11), 6099−6107.

(18) Ben Yaacov, A.; Ben David, R.; Grinter, D. C.; Held, G.; Eren, B. Identification of Adsorbed Species and Surface Chemical State on Ag(111) in the Presence of Ethylene and Oxygen Studied with Infrared and X-Ray Spectroscopies. *Physchem* **2021**, *1* (3), 259−271.

(19) Grass, M. E.; Karlsson, P. G.; Aksoy, F.; Lundqvist, M.; Wannberg, B.; Mun, B. S.; Hussain, Z.; Liu, Z. New Ambient Pressure Photoemission Endstation at Advanced Light Source Beamline 9.3.2. *Rev. Sci. Instrum.* **2010**, *81* (5), 053106.

Downloaded from pubs.acs.org/jpccck/article-pdf/130/31/10952/6254925/acs.jpcc.6c04216.pdf by guest on 11 November 2026

(20) Eren, B.; Salmeron, M. Beam-Induced Effects in Ambient Pressure Experiments with X-Rays. *In Ambient Pressure Spectroscopy in Complex Chemical Environments*; American Chemical Society, 2021; *1396*, 249, 265,
(21) Heine, C.; Lechner, B. A. J.; Bluhm, H.; Salmeron, M. Recycling of CO_2: Probing the Chemical State of the Ni(111) Surface during the Methanation Reaction with Ambient-Pressure X-Ray Photoelectron Spectroscopy. *J. Am. Chem. Soc.* **2016**, *138* (40), 13246−13252.
(22) Takagi, N.; Yoshinobu, J.; Kawai, M. Temporal and Local Reduction of a Potential Energy Well under Dynamic Equilibrium: CO on Ni(100). *Phys. Rev. Lett.* **1994**, *73* (2), 292−295.
(23) Lauterbach, J.; Wittmann, M.; Küppers, J. Adsorption of CO at Ni(100) Surfaces: A FTIRAS - TDS Study. *Surf. Sci.* **1992**, *279* (3), 287−296.
(24) Glass, A. S.; Bermudez, V. M. Infrared Study of High Pressure and High Temperature Coadsorption of CO and H_2 on Clean and on Carbided Ni(100). *J. Vac. Sci. Technol., A* **1990**, *8* (3), 2622−2626.
(25) Mohsenzadeh, A.; Richards, T.; Bolton, K. DFT Study of the Water Gas Shift Reaction on Ni(111), Ni(100) and Ni(110) Surfaces. *Surf. Sci.* **2016**, *644*, 53−63.
(26) Mac Rae, A. U. Adsorption of Oxygen on the {111}, {100} and {110} Surfaces of Clean Nickel. *Surf. Sci.* **1964**, *1* (4), 319−348.
(27) Hardegree, E. L.; Ho, P.; White, J. M. Sulfur Adsorption on Ni(100) and Its Effect on CO Chemisorption: I. TDS, AES and Work Function Results. *Surf. Sci.* **1986**, *165* (2−3), 488−506.
(28) Mohsenzadeh, A.; Bolton, K.; Richards, T. DFT Study of the Adsorption and Dissociation of Water on Ni(111), Ni(110) and Ni(100) Surfaces. *Surf. Sci.* **2014**, *627*, 1−10.
(29) Hoeft, J. T.; Polcik, M.; Sayago, D. I.; Kittel, M.; Terborg, R.; Toomes, R. L.; Robinson, J.; Woodruff, D. P.; Pascal, M.; Nisbet, G.; Lamont, C. L. A. Local Adsorption Sites and Bondlength Changes in Ni(1 0 0)/H/CO and Ni(1 0 0)/CO. *Surf. Sci.* **2003**, *540* (2−3), 441−456.
(30) Li, J.; Schiøtt, B.; Hoffmann, R.; Proserpio, D. M. Coadsorption of Carbon Monoxide and Hydrogen on the Ni(100) Surface: A Theoretical Investigation of Site Preferences and Surface Bonding. *J. Phys. Chem.* **1990**, *94* (4), 1554−1564.
(31) Trenary, M.; Uram, K. J.; Bozso, F.; Yates, J. T. Temperature Dependence of the Vibrational Lineshape of CO Chemisorbed on the Ni(111) Surface. *Surf. Sci.* **1984**, *146* (1), 269−280.
(32) Kumari, S.; Deshpande, P. A. Density Functional Theory Analysis of the Stability of H_2O and CO_2-Derived Surface Species over Low-Index Ni Facets. *Appl. Surf. Sci.* **2024**, *669*, 160375.
(33) Wei, M.; Fu, Q.; Yang, Y.; Wei, W.; Crumlin, E.; Bluhm, H.; Bao, X. Modulation of Surface Chemistry of CO on Ni(111) by Surface Graphene and Carbidic Carbon. *J. Phys. Chem. C* **2015**, *119* (24), 13590−13597.
(34) Weatherup, R. S.; Amara, H.; Blume, R.; Dlubak, B.; Bayer, B. C.; Diarra, M.; Bahri, M.; Cabrero-Vilatela, A.; Caneva, S.; Kidambi, P. R.; Martin, M. B.; Deranlot, C.; Seneor, P.; Schloegl, R.; Ducastelle, F.; Bichara, C.; Hofmann, S. Interdependency of Subsurface Carbon Distribution and Graphene-Catalyst Interaction. *J. Am. Chem. Soc.* **2014**, *136* (39), 13698−13708.
(35) Wiltner, A.; Linsmeier, C. Thermally Induced Reaction and Diffusion of Carbon Films on Ni(1 1 1) and Ni(1 0 0). *Surf. Sci.* **2008**, *602* (23), 3623−3631.

Downloaded from pubs.acs.org/jpccck/article-pdf/130/31/10952/6254925/acs.jpcc.6c04216.pdf by guest on 11 November 2026

https://doi.org/10.1021/acs.jpcc.6c04216
J. Phys. Chem. C 2026, 130, 10952−10957